Tribology International 212 (2025) 110977

Contents lists available at ScienceDirect

Tribology International

journal homepage: www.elsevier.com/locate/triboint

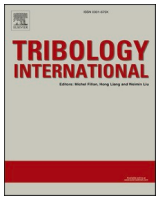

Full length article

Production and characterization of texture in PCD cutting tools with femtosecond laser: Analysis of texture quality and surface integrity in the turning of AA2011-T4 aluminum

Felipe Chagas Rodrigues de Souza [a,*], Wagner de Rossi [b], Leonardo Rosa Ribeiro da Silva [a,c], Fábio Rüstow de Paula [c], Álisson Rocha Machado [a,c,**]

[a] Federal University of Uberlandia, Av. João Naves ďAvila, 2121, Uberlândia MG, 38400-902, Brazil
[b] Centro de Lasers e Aplicações, Instituto de Pesquisas Energéticas e Nucleares, São Paulo 05508-000, Brazil
[c] Mechanical Engineering Graduate Program, Pontifícia Universidade Católica do Paraná – PUCPR, Rua Imaculada Conceição, 1155, Curitiba, PR 80215-901, Brazil

ARTICLE INFO

Keywords:
Laser texturing
Femtosecond laser
PCD tools
AA2011-T4 aluminum
MoS_2 microparticles
Roughness

ABSTRACT

This study investigates the creation of textures on polycrystalline diamond (PCD) cutting tools using femtosecond laser processing and evaluates the influence of these textures on the turning of AA2011-T4 aluminum alloy. Four types of linear textures with varying orientations and dimensions were developed, and their quality was assessed through 3D profilometry and energy-dispersive spectroscopy (EDS). The turning tests evaluated the surface roughness of the machined workpiece, material adhesion on the tool, and the effect of incorporating solid lubricant microparticles (MoS_2) into the textures. The results indicate that femtosecond laser texturing was effective, causing no thermal damage or graphitization of the PCD. During machining, textures oriented perpendicular to the cutting edge reduced aluminum adhesion and lead to better surface finish. In contrast, textures parallel to the cutting edge intensified material anchoring, increasing the risk of tool structure failure. The use of MoS_2 decreased material retention within the textures, facilitated chip evacuation, and contributed to improved machining performance. The greatest reduction in roughness (49 %) was observed for larger perpendicular textures combined with MoS_2. Additionally, larger textures demonstrated superior performance by promoting chip segmentation and reducing thermal effects. The results demonstrate that femtosecond laser texturing is a viable technique for optimizing the performance of cutting tools in the turning of aluminum alloys, enhancing the surface quality of the machined part, and reducing tool wear.

1. Introduction

Surface texturing refers to the creation of topographical patterns capable of altering the interaction of the surface compared to a flat, smooth one, such that its presence can enhance the tribological performance of the system in which the surface participates. When applied to cutting tool surfaces, textures can modify the tribological phenomena at the workpiece/chip-tool interface, thereby influencing tribological performance and chip formation behavior [1].

Several methods are available for producing textures on tools, each with its own advantages and disadvantages. With technological advancements, some methods have been refined and made more cost-effective, becoming predominant for this purpose. As noted in the review by Machado et al. [2], two methods have emerged as the most prevalent for producing textured tools in recent years: Electrical Discharge Machining (EDM), accounting for 19 % of all articles reviewed during the evaluated period (2018–2021), and Laser (Light Amplification by Stimulated Emission of Radiation), representing 65 %. Samad et al. [3] also suggest that ultrashort pulse lasers are a significant trend for tool texturing due to their high repeatability without damaging the textured surface.

Laser machining is a non-conventional process where chip generation is minimal, with material being removed in the form of vaporized matter. The principle behind most lasers involves an orbital electron of

* Corresponding author.
** Corresponding author at: Federal University of Uberlandia, Av. João Naves ďAvila, 2121, Uberlândia MG, 38400-902, Brazil.
E-mail addresses: felipechagas@ufu.br (F.C.R. de Souza), wderossi@ipen.br (W. de Rossi), leorrs@ufu.br (L.R.R. da Silva), fabio.rustow@pucpr.edu.br (F.R. de Paula), alisson.rocha@pucpr.br (Á.R. Machado).

https://doi.org/10.1016/j.triboint.2025.110977
Received 20 May 2025; Received in revised form 30 June 2025; Accepted 5 July 2025
Available online 7 July 2025

an atom or molecule jumping to a higher energy level upon absorbing a quantum of energy. Upon returning to its natural state, this energy is released as light with photon energy lower than that absorbed by the electron. Consequently, laser emission exhibits a highly defined wavelength (monochromatic), high collimation, and high phase coherence among photons.

The choice of lasers has gained popularity due to their advantages in texture production, such as high precision and reproducibility. In the context of micromachining, diverse types of lasers are available for different applications. Excimer lasers are more suitable for working with polymers and ceramics, while Nd:YAG lasers are recommended for marking and drilling. For micromachining metals, it is essential for the laser to be pulsed, with pulse durations in the range of microseconds, nanoseconds, or even shorter, as this parameter is directly correlated with thermal and mechanical damage such as burrs, cracks, structural changes [4,5].

A type of laser capable of micromachining while addressing these concerns is the ultrafast pulsed laser, with pulses in the range of tens or hundreds of femtoseconds (1 fs = 10^{-15} s). It can process a wide variety of materials (metals, polymers, ceramics, semiconductors) without causing significant thermal or mechanical damage to the workpiece. The femtosecond laser is an ultrafast pulsed laser where heat transfer is so insignificant that it can even cut explosive materials, as it does not induce significant thermal exchange or shock waves to the point of ignition [6]. Due to these characteristics, this laser has gained popularity in research applications, industries, and even fields beyond engineering, such as medicine. However, several other factors need to be considered when choosing a laser, such as cost, reliability, processing capabilities, and performance.

The ablation effect (for solid materials), typical of femtosecond lasers, involves energy in the range of 10^{1} a 10^{2} μJ. When these types of pulses are directed at the material, the duration of this incidence is shorter than the vibrational period of the material's ionic lattice. Consequently, most of the pulse energy will be absorbed by the electrons, heating them. However, before bond rupture occurs, lattice heating may generate a small Heat-Affected Zone (HAZ), which can be controlled and even minimized when the irradiation parameters are appropriate for the material being processed [3].

Fork et al. [7] pioneered the application of ultrafast pulsed lasers to polycrystalline diamond (PCD), using pulses of less than 0.1 ps. Since diamond is a non-metallic material, the presence of free electrons on the surface is due to the excitation of valence electrons caused by the laser's multiphoton ionization effect [8,9]. It is important to note that natural diamonds are transparent and, as mentioned earlier, are challenging to machines with conventional lasers. However, PCDs are opaque and, along with their thermal properties, are favorable for laser machining.

Examples of parameters for machining PCD using femtosecond lasers have been studied in articles such as [10,11]. Sotillo et al. [11], in their work on producing linear textures, concluded that a high-frequency laser (500 kHz) significantly reduces the graphitization effect compared to lower frequencies (such as 5 and 50 kHz) and also improves the Ra parameter on the sample surface. This conclusion was also replicated in other studies [12], which conducted a similar investigation but focused on dimple-type textures.

Although PCD is an extremely hard material, it also stands out for its low electrical conductivity, characteristics that are irrelevant for laser-based processes. In electrical discharge machining (EDM), the process is hindered by the material's low electrical conductivity. Unlike natural diamonds, PCD contains a small amount of cobalt, which provides some electrical conductivity, albeit low. In laser cutting, however, material removal occurs through thermal melting and vaporization without mechanical contact, being influenced mainly by beam absorption and thermal conductivity. This allows the cutting of materials regardless of hardness or electrical conductivity, as long as the material effectively absorbs the laser energy.

The ease of post-processing with femtosecond lasers proves to be an advantageous application of this type of laser. Other types of long-pulse lasers can fuse debris within the textures, requiring more rigorous surface cleaning methods, including, in some cases, micro-grinding [13].

One way to enhance the benefits of texturing in a cutting tool is the simultaneous use of solid lubricants, which together can reduce the loads required to shear the material from the workpiece. Several studies have shown that solid lubricants in textured tools have had a significant impact on improving friction and reducing cutting forces [14,15].

These types of lubricants possess lamellar microstructures with low adhesion forces between them. These lamellae exhibit low resistance to each other and shear easily, acting as an efficient lubricating film with a relatively low coefficient of friction. A disadvantage is the low durability of solid lubricants on the flat surfaces of cutting tools, but this can be compensated for by combining their use with textured tools [16]. In this way, the textures on cutting tools, along with their ability to store debris, can accommodate solid lubricants. The mechanism, as described by Feng et al. [17], operates as follows: the texture is initially filled with the solid lubricant, and during the machining process, the heavier debris from the chips gets trapped within the textures. Then, the solid lubricant overflows, forming a lubricating film layer on the textured surface.

For groove-type textures, linear ones are more efficient for machining with solid lubricants compared to patterned grooves [18]. In dimple-type textures, efficiency lies in the formation of a discontinuous lubricating film that helps reduce temperature [19]. However, according to Sun et al. [20], the most effective method for working with solid lubricants is with hybrid geometries (grooves and dimples). In the study conducted by Gajrani et al. [21], which involved turning AISI 1040 steel, it was found that in the presence of MoS_2 in the texture, the average roughness value decreased by 2–11 %, and the average temperature value decreased by 4–20 % compared to a texture without such filling.

In machining, aluminum is known for its high machinability, allowing it to be machined at extremely high cutting speeds (up to 5 times higher than steel). However, it has a low modulus of elasticity (on average 1/3 that of steel) and high ductility, which generates continuous chips that strongly adhere to cutting tools [22]. Aluminum-copper alloys (series 2XXX) are generally complex due to the considerable number of additives used to increase corrosion or structural resistance and control grain structure. They are characterized by good mechanical strength (resulting from precipitation hardening that occurs after solution heat treatment) and good machinability. The AA2011-T4 alloy is commonly used in household appliance parts, automotive finishes, and artillery components. Its hardness, due to heat treatment, is around 100 HV, and its tensile and shear strengths are respectively 310 MPa and 190 MPa [23]. For machining aluminum alloys, PCD is the most recommended tool material due to its excellent hardness and low coefficient of friction against this work material.

Thus, the main objective of the present work is to define suitable femtosecond laser parameters for producing textures on PCD cutting tools and to evaluate the feasibility of using distinct types of textures during the turning of AA2011-T4 aluminum alloy. The turning evaluation was conducted by measuring the roughness on the turned parts, a key output variable for analyzing process quality, especially in finishing operations on aluminum alloys. Additionally, the quality of the produced texture and the impact of using solid lubricant on the considered textures will be observed.

2. Methodology

2.1. Texture production and evaluation

Studies such as those by Yang et al. [24,25] provide a clear correlation regarding the influence of each texture parameter (size, distance from the cutting edge, density, and depth) on machining, focusing solely on dimple-type textures. In contrast, this project uses only groove-type textures, following authors like Kang et al. [26], who indicated that this is one of the best texture geometries for aluminum turning. Authors

such as Wu et al. [27] even found an optimal relationship between width and depth for groove textures, but in the context of carbon steel machining.

Furthermore, linear grooves demonstrated the best performance for solid lubricant action, as observed in the study by Orra e Choudhury [18]. Regarding groove direction, there are discrepancies among different authors. Kumar e Patel [28] and Grguraš e Pušavec [29] concluded that a more favorable direction for machining (in terms of cutting forces) is parallel to the cutting edge (perpendicular to chip flow), whereas in Su et al [30] study (which machined Ti6Al4V), the conclusion was the opposite. However, it is worth noting that the materials studied by these authors are quite different, with the first two machining high-carbon and chromium steel [28] and medium-carbon structural steel [29], respectively, while the latter [30] machined Ti6Al4V, meaning none worked with a material as ductile as aluminum.

After these observations, the need for further investigation became evident. It is crucial to explore the effect of groove directions in machining highly ductile materials and to determine the best dimensions for such textures. Articles that produced textures on PCD, such as [30–32], highlighted that few studies on PCD tools venture into producing textures beyond the dimensions already explored in other works. The only exception found is the study by Ghosh e Pacella [33], but for very small textures. Consequently, it is challenging to anticipate a trend for optimal texture dimensions. Therefore, there is a need to create textures with intermediate and/or larger dimensions compared to those already studied in published works.

Although several studies in the literature have investigated PCD textured tools for aluminum machining, most of them employ similar texture dimensions (typically around 80 μm in width and depth, with spacings between 60 and 100 μm). Based on a systematic review conducted by the authors [2], it was identified that edge cases (the boundaries of the dimensional range) remain underexplored. Therefore, this work deliberately selected combinations representing the lower and upper limits observed in the literature to assess potential behavioral trends over a broader dimensional span.

It is important to note that the “texture dimension” factor in this study encompasses four distinct geometrical parameters: groove width, groove depth, inter-groove spacing, and the distance from the cutting edge to the start of the textured region. This methodological grouping was adopted to maintain a balanced number of geometrical and operational variables (cutting speed and lubrication), ensuring a feasible experimental design while preserving the ability to analyze major effects. For studies aiming at precise geometric optimization, a complete breakdown of these variables is advisable, enabling a robust factorial analysis.

Authors such as [30,31], and [32], who also investigated textures on PCD tools, employed groove-type textures with widths of 60 μm and spacing close to 85 μm. This dimensional range has been extensively explored in the literature. Therefore, in the present work, an effort was made to go beyond the commonly studied values. Considering an interval of approximately ±40 μm around the referenced spacing, texture sizes of 45 μm and 120 μm (rounded values) were selected. These dimensions have not yet been addressed in the literature and represent an unexplored range. It is important to highlight that PCD tools are expensive, and given the available resources, it was necessary to define textures that would both extend beyond known references and offer novelties. The results obtained in this study may help determine whether there is an optimal texture size within this new range or whether such an optimum lies beyond it. Thus, two types of textures were chosen: 45 and 120 μm (depth equal to width), as these are intermediate values compared to those used in similar investigations which also studied cutting tools with PCD material [30–32].

The distance from the cutting edge where the textures begin is a parameter rarely discussed in literature. Therefore, considering the small area of PCD available on the surface of cutting tools and the relatively low machining depth (2 mm), it was decided to produce all textures starting at 120 μm from the cutting edge. This value approximates those found in the few studies where this dimension was mentioned [31]. Additionally, it is a multiple of the selected values for the texture width and spacing, facilitating the design and production of textures. This ensures that the contact area between the chip and the tool will certainly be within the textured surface region, considering the expected chip-tool contact length, which is a function of machining variables such as the depth of cut, the feed rate, and the rake angle of the cutting tool.

In the same sense as the distance from the cutting edge variable, the spacing of all grooves was set at 120 μm. The directions under investigation are grooves parallel and perpendicular to the cutting edge. Thus, four distinct types of textures were created on the rake surface of the cutting tool, as described in Table 1.

The textures were produced using a femtosecond laser (ultrashort pulses) of Ti:sapphire, model "Element PRO 400" from Femtolasers Produktions GmbH, amplified by the "Femtopower Double 10 kHz" system, also from Femtolasers. In addition to the base articles for defining the dimensions of the textures, specific articles were studied for selecting laser parameters in the production of textures on PCD [10,34,35], which also helped to prevent the occurrence of graphitization on the material. In pre-tests using PCD plates, the laser was properly calibrated. The laser beam was polarized, set with emission centered at 800 nm, a temporal width of 30 fs, maximum pulse energy of 200 μJ, and a repetition rate of 10 kHz. For the machining process, the laser beam was injected into a workstation model "PRJ0221-Femtolasers" from Laser Engineering Applications, guiding the beam to the focusing lens. In this system, the focal point remains stationary, and the sample is moved by an Aerotech three-axis translation stage, series ANT130, with a precision of approximately 10 nm. The movement programming is conducted using the Mastercam 2018 - Mill software with a dedicated post-processor for the laser system. When focused with an f = 20 mm lens, the focal spot diameter is approximately 3.6 μm. Table 2 summarizes the main parameters mentioned above.

The PCD diamond textures were evaluated through a multidisciplinary approach, combining different characterization techniques. The chemical composition was analyzed through Energy Dispersive Spectroscopy (EDS) in a Scanning Electron Microscope (SEM), allowing verification of the presence of elements indicative of graphitization. EDS in SEM is a technique that uses the interaction of X-rays generated by an electron beam with the sample to provide information about the elemental composition of the material, allowing the identification of the elements present with high precision, although quantitative analyses are not exact. For this spectroscopy, 3 spectra were evaluated in different regions of 3 cutting tools, for 2 batches of tools: smooth (non-textured) and textured tools. A 3D profilometry was conducted using MountainsMap software to verify the produced dimensions and ensure they aligned with the expected average values consistent with the laser precision (focusing on depth, width, and spacing of the textures), enabling detailed analysis of the topographic variations resulting from irradiation. For width measurement, this was conducted at a depth of 15–20 % of the total depth, considering the rounding of the groove edge. Finally, structural integrity is examined with the aid of an optical and an electronic microscope, allowing the identification of possible cracks or fissures generated by the efforts or vibrations during the turning process.

Table 1
Types of linear groove textures on PCD.

Texture	Direction (relative to the cutting edge)	Depth and Width (μm)
PA45	Parallel	45
PE45	Perpendicular	45
PA120	Parallel	120
PE120	Perpendicular	120

Table 2
Typical parameters of the femtosecond laser used to create textures on PCD.

Parameter	Value
Pulse width	30 fs
Wavelength	800 nm
Focal spot diameter	3.6 μm
Maximum pulse energy	200 μJ
Pulse repetition rate	10 kHz

2.2. Application of solid lubricant on textures

The solid lubricant chosen for this project is molybdenum disulfide powder (MoS_2). The particles of this powder have diameters of up to 5 μm and a thickness of approximately 1 nm, allowing them to easily fill the textures. The application of MoS_2 was initially performed using a brush on the textures, followed by a mixture of sealant with additional lubricant. It is important to note that before applying the lubricant, the textures were cleaned to remove any debris, as recommended by Zalloum et al. [36] and Kononenko et al. [37]. The textures were cleaned through brushing with bristles smaller than the width of the textures and also by ultrasonic cleaning, which operates via cavitation bubbles.

The proportion of this mixture was the maximum dilution of the powder that the sealant allowed for saturation without losing its consistency (approximately 4 parts of sealant to 1 part of MoS_2), optimizing the desired effect. The applied sealant was OrbiVed337 silicone, with resistance to temperatures up to 320°C.

Due to laboratory limitations, it was not possible to apply MoS_2 as a coating fixed directly to the textured surface, which would be the ideal solution for industrial applications. In this work, the strategy adopted was to use silicone sealant as a medium to retain the MoS_2 powder within the grooves, allowing the lubricant to remain embedded during machining.

It is important to highlight that the primary objective of applying MoS_2 in this study was not to reduce the friction coefficient between the chip and the tool surface, but rather to prevent chip stagnation and the anchoring effect of aluminum chips inside the textures (which is being discussed in more detail in item 3.2). Aluminum is a highly ductile material that deforms according to the tool's surface geometry, allowing the chip to penetrate and embed itself into the textured grooves. This can generate substantial stress on the tool surface, potentially leading to premature damage or failure.

The chosen ratio of 20 % MoS_2 to silicone is relatively high but remains viable. Higher concentrations, such as 30–40 %, tend to compromise the elasticity of the silicone matrix, increasing the risk of cracking under continuous mechanical flexing [38]. Based on data from similar composite materials (silicone matrices with solid lubricant fillers), a concentration of 20 % MoS_2 is expected to reduce the coefficient of friction by approximately 40–60 %, depending on dispersion quality, which corresponds to an estimated friction coefficient of approximately 0.3 [38].

Fig. 1 shows a rake face of a textured cutting tool with PE45-type texture (depth and width of 45 μm). In the left image, the texture is empty; in the center image, the texture contains only the solid lubricant; and in the right image, the texture is filled with a mixture of lubricant and sealant, the latter being the condition selected for this work.

2.3. Cutting parameters for turning

The cylindrical turning experimental tests were conducted in a CNC lathe machine, model Multiplic 35D, manufactured by Romi S.A., with variable spindle speed from 0 to 3000 rpm and 11 kW of power. The aluminum workpieces were rigidly clamped using a chuck and supported at the opposite end with a tailstock to ensure stability during machining.

For the experiments, a series of articles on turning aluminum with textured tools were considered to determine possible cutting conditions for this material. These studies analyzed aluminum turning using groove-type textures on the rake face of the cutting tool [26,33,39–43]. During pre-tests, it was observed that a 15-second run is sufficient to stabilize the cutting force and temperature parameters. Given the negligible wear rate between PCD and aluminum, the test run was set to 15 s, with cutting speeds of 200 m/min and 400 m/min, on an aluminum alloy AA2011 T4 bar with a diameter of 60 mm and a length of 600 mm. The depth of cut and feed rate were set to 2 mm and 0.2 mm/rev, respectively. These values are commonly used in industrial operations and are close to those reported in the articles cited at the beginning of this section.

The work material is an aluminum alloy AA2011-T4, composed of aluminum (balance), copper (up to 6 %), iron (up to 0.7 %), silicon (5–6 %), zinc (~0.3 %), and, in some cases (as in this study), small amounts of lead and bismuth (0.9 % combined) to improve machinability. The presence of Bi and Pb, insoluble elements that appear in the matrix as globules, enhances machinability. The phases after solidification and heat treatment consist of Al-Cu with Fe, Pb, and Bi (insoluble) [44]. The 'T4' designation indicates a thermal solution treatment (1–4 h at 495°C – 530°C, followed by rapid cooling to room temperature in water) and natural aging (4–5 days at room temperature). Its hardness is 95 HV, and its fatigue, tensile, and shear strengths are 75, 310, and 190 MPa, respectively [23].

The cutting tool material is polycrystalline diamond (PCD), which exhibits significantly higher toughness compared to monocrystalline diamond and is proportional to the grain size of the material [45]. A limitation of PCD is its application at elevated temperatures: when machining exceeds approximately 780°C (as typically occurs in machining ferrous materials), PCD begins to graphitize. The main advantages of PCD as cutting tools for aluminum machining include extended tool life (designed to operate for months), high-speed

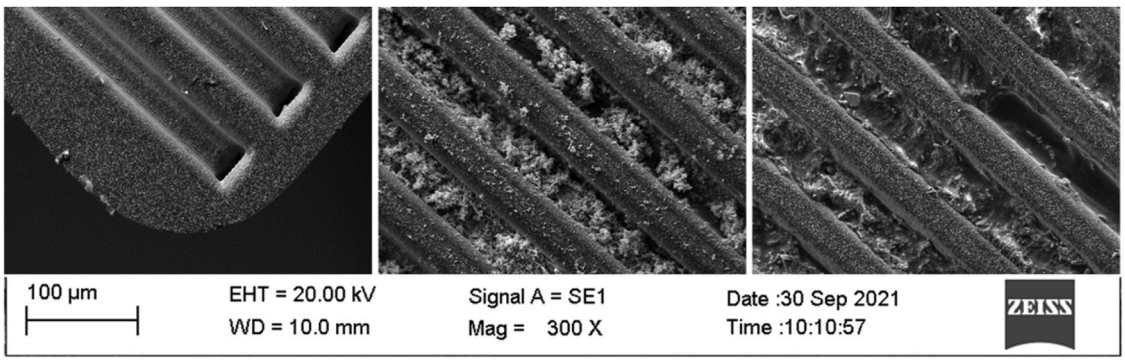

Fig. 1. From left to right, there is a sequence of solid lubricant application on the texture. Initially, without lubricant application, then filled with MoS_2, and finally with the mixture of sealant and lubricant.

performance (capable of operating up to 10 times faster than carbide tools at maximum efficiency and effectiveness), and superior surface finish quality. The inserts are designated ISO CPGW120404F01N-0AA, manufactured by Mapal. A special tool holder was used, and when an insert is mounted, the following geometry is produced: side cutting edge angle of −5°, final cutting edge angle of 15°, back rake angle of 6.5°, side rake angle of 6.5°, and clearance angle of 4.5°.

The combination of PCD tools and aluminum machining does not typically result in significant tool wear over time, as PCD is an extremely hard material and aluminum is highly ductile. In fact, PCD tools are specifically designed to operate for months in machining applications, particularly when cutting non-ferrous materials like aluminum, as highlighted by [45]. Given this exceptionally low wear behavior, conducting tool life tests in this context would be inefficient and impractical, as it would require excessive amounts of material without offering proportional insight [46].

Instead, the durability of the laser-textured surface is more directly linked to the structural integrity of the PCD after irradiation. The laser-produced grooves may act as stress concentrators and, under certain machining conditions, initiate crack propagation that compromises the tool's integrity. Therefore, this study prioritized the evaluation of whether the selected texture dimensions could structurally withstand the imposed cutting parameters (cutting speed, feed rate, and depth of cut), rather than focusing on progressive tool wear over time.

2.4. Analysis of surface roughness of the machined workpiece

Surface roughness analysis plays a fundamental role in evaluating the quality of machined parts and optimizing the manufacturing process. Roughness directly affects dimensional accuracy, wear, friction, and lubrication, influencing the part's performance in mechanical applications. During turning operations, factors such as cutting speed, feed rate, and depth of cut determine the surface finish. Surfaces with excessive roughness can compromise the part's strength and increase the need for rework, while excessively smooth surfaces may hinder lubricant retention. Therefore, adjusting roughness based on the application improves component durability and efficiency.

For each tested condition, three measurements were taken using the Taylor Hobson S-128 profilometer, spaced 120° apart by rotating the bar on each of the turned surfaces during the tests. The measurement was carried out directly on the lathe, without handling the bar, in order to avoid any alteration of the roughness of the machined surface. A Gaussian filter (cut-off) of 0.8 mm, a field of 100 μm, and a measurement path length (Lm) of 4 mm were employed. The analyzed parameters were Ra, Rq, and Rz. Data processing was performed using the Taly-Profile Lite software.

2.5. Statistical analysis

Given the number of available cutting edges, the tests were configured using a fractional factorial design of type 2^{4-1}. Table 3 details the parameters of the conditions studied. To avoid interference from the order of results, the experiments were conducted randomly. A total of 8 distinct cutting conditions were tested, with 3 repetitions for each condition, resulting in 24 trials. It is important to note that, in addition to the combinations of tests listed in Table 3, smooth tools (without textures) were also tested under the same machining conditions. It is worth mentioning that the direction of the textures is referenced relative to the cutting edge of the tool.

Table 3
Experimental design matrix for fractional factorial 2^{4-1}.

Test Condition	Texture Direction	Texture Depth/ Width (μm)	Cutting Speed (m/ min)	Lubrication Condition
1	Parallel	45	400	Dry
2	Perpendicular	45	400	With MoS_2
3	Parallel	120	400	With MoS_2
4	Perpendicular	120	400	Dry
5	Parallel	45	200	With MoS_2
6	Perpendicular	45	200	Dry
7	Parallel	120	200	Dry
8	Perpendicular	120	200	With MoS_2

The experimental results were analyzed using Statistica® software, with a confidence level of 95 %. Initially, an analysis of variance (ANOVA) was performed to assess the significance of the parameters and analyze the data obtained from the experiments. This made it possible to generate a Pareto chart, which indicates the significance of each parameter studied on the surface roughness of the workpiece.

For the analysis of the machined surface roughness, the parameters *Ra*, *Rq*, and *Rz* were evaluated to compare smooth tools with the textured ones. In the Pareto analysis for surface roughness, only the *Ra* parameter is presented, as all roughness parameters followed the same trend and proportion in the results.

3. Results and discussion

3.1. Tool texturing

The four types of textures were successfully produced on the rake faces of PCD cutting tools, covering an area of approximately 10 mm^2. Fig. 2 illustrates these four types of textures. The primary cutting edge used as a reference for turning is the edge located on the right side of the images.

As observed in Fig. 2, the textures are almost free of debris, especially for the 120 μm textures (types PA120 and PE120). As described in Section 2.2, any debris was removed manually using a fine-bristle brush and diamond paste. Additionally, it was verified that no cracks or fissures were generated by the laser.

A profilometry analysis conducted on the textures of types PA45 and PE45 revealed that the error in both depth and width of the texture varied around ±5 μm. The cross-sectional profile of the texture indicates that they are not perfectly square; the width starts at the intended value and tapers along the depth. At the maximum depth point (the intended texture depth), the width measures approximately half the intended width (Fig. 3).

Fig. 5 and Fig. 6 display the 3D textures generated from the profilometry analysis. In these figures, the markings that originated the cross-sectional cuts providing the graphs in the previous figures (Fig. 3 and Fig. 4) are visible. They demonstrate the high quality of textures produced by the femtosecond laser. No debris is present in the analyzed regions, and surface imperfections consist only of impurities originally present in the PCD.

It is particularly noticeable in Fig. 6 that the texture depth increases toward the end of the groove (last 0.5 mm), which is expected since, at this point, the beam movement slows down, operating for a slightly longer fraction of time. For textures with a depth of 45 μm, this increase was about 11 %, and for 120 μm, it was 25 %. The amplitude curve of the height profile (on the right side of the figure) indicates a significant depth of up to 150 μm. However, this occurs because the graph generated for this texture focuses on the region at the end of the groove. This does not happen in Fig. 5 because, for the 45 μm textures, the evaluated region is relatively far from the end of the groove.

Using Energy-Dispersive X-ray Spectroscopy (EDS) coupled with a Scanning Electron Microscope (SEM), a detailed analysis of the polycrystalline diamond (PCD) material was performed before and after femtosecond laser irradiation.

To evaluate potential structural changes in the PCD due to femtosecond laser exposure, the material samples were divided into two groups: one analyzed before laser irradiation and the other after. Femtosecond laser irradiation, known for its ability to induce localized changes in materials, was applied under controlled conditions, and its

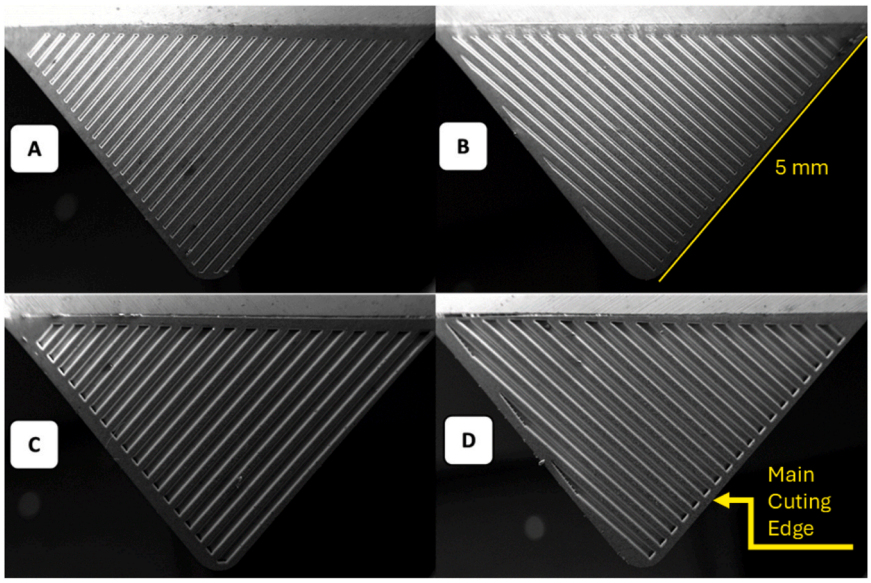

Fig. 2. Types of textures produced on the PCD cutting tool inserts. A: grooves parallel to the main cutting edge with a width and depth of 45 μm. B: grooves perpendicular to the main cutting edge with a width and depth of 45 μm. C: grooves parallel to the main cutting edge with a width and depth of 120 μm. D: grooves perpendicular to the cutting edge with a width and depth of 120 μm.

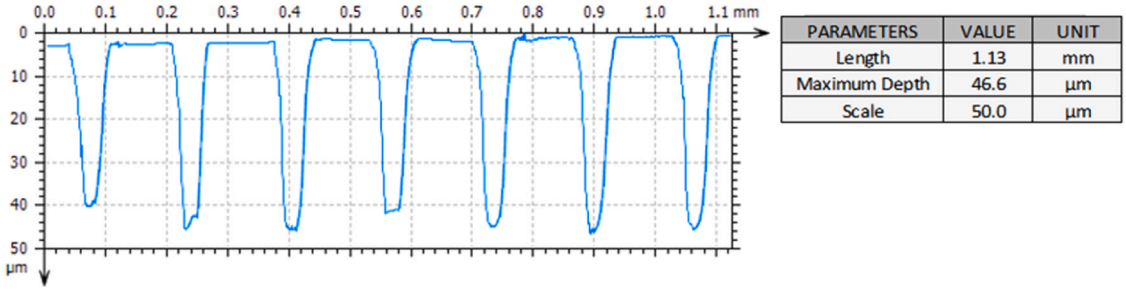

PARAMETERS	VALUE	UNIT
Length	1.13	mm
Maximum Depth	46.6	μm
Scale	50.0	μm

Fig. 3. Cross-sectional profile of a 45 μm texture (types PA45 and PE45).

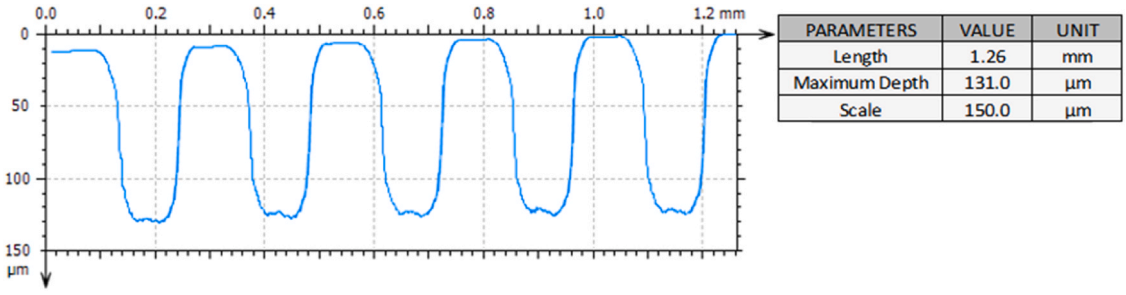

PARAMETERS	VALUE	UNIT
Length	1.26	mm
Maximum Depth	131.0	μm
Scale	150.0	μm

Fig. 4. Cross-sectional profile of a 120 μm texture (types PA120 and PE120).

influence on the structure and composition of the PCD diamond was analyzed.

A comparison of EDS results between samples before and after laser application indicated no significant graphitization of the material. Table 4 presents the average weight percentages of the chemical elements detected in each condition (before and after laser irradiation). Graphitization of PCD diamond refers to the transformation of carbon from a diamond structure into a more amorphous graphite structure. Although EDS cannot directly identify graphitization, as it does not distinguish between carbon allotropes (such as sp^3 in diamond and sp^2 in graphite), a pronounced structural transformation would likely affect the surface's affinity for oxygen, potentially causing a noticeable reduction in the oxygen content — which was not observed. Therefore, the stable proportion between C and O suggests that the PCD structure was largely preserved after laser interaction. Nonetheless, this remains an indirect indication, and the use of complementary techniques such as Raman spectroscopy is recommended for a conclusive evaluation of the crystalline structure.

Tungsten (W) is not part of the PCD composition but is detected because the cutting tool body is made of cemented carbide, with the PCD plate being a thin layer on a small surface area. Tungsten from the cemented carbide (WC-Co) is detected in massive quantities. It is worth noting that tungsten is 15 times heavier than carbon, and the percentages presented are based on weight.

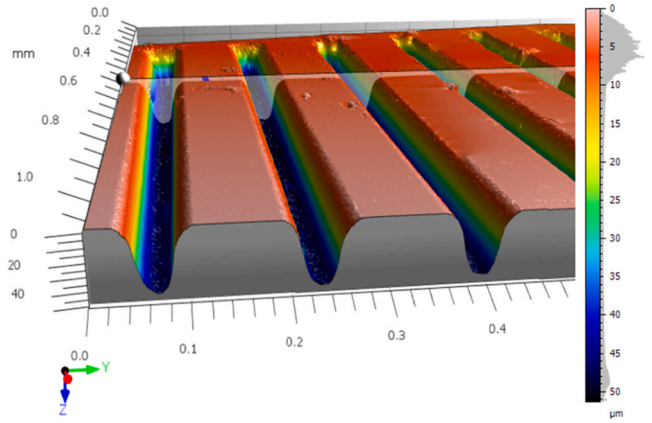

Fig. 5. 3D graph of the profile of a texture with dimensions of 45 µm.

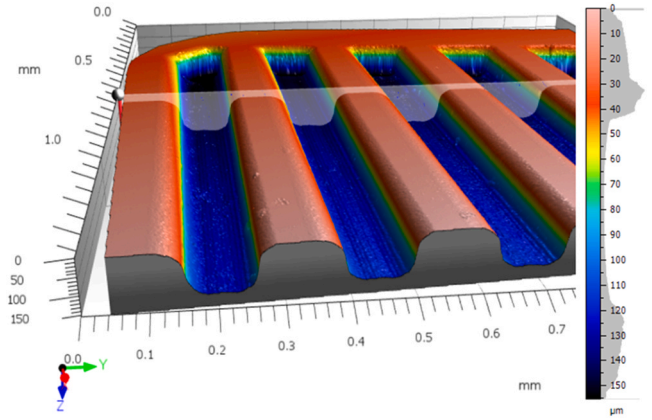

Fig. 6. 3D graph of the profile of a texture with dimensions of 120 µm.

Table 4
Comparison of the average chemical composition of the PCD cutting tool surface before and after femtosecond laser irradiation (all results in weight percentages).

Elements	C (Carbon)	Co (Cobalt)	W (Tungsten)	O (Oxygen)
Before Laser	79.94	6.20	12.75	1.11
After Laser	79.65	5.82	13.26	1.27

Fig. 7 (on the right) illustrates the EDS analysis of the cutting tool surface before and after the femtosecond laser irradiation. The spectra are very similar. The post-texturing EDS analysis was performed within a texture composed of grooves parallel to the cutting edge, with a groove width of 120 µm. The center of the analyzed region was located 180 µm from the main cutting edge, covering an area of 30 × 60 µm, with the 60 µm dimension aligned parallel to the groove direction. Fig. 7 (on the left) presents the scanning electron microscopy (SEM) image with a clear indication of the analyzed area. For comparison purposes, the pre-texturing EDS analysis was carried out in the same location, but on a non-textured tool, allowing direct evaluation of the compositional changes promoted by the laser texturing process.

Additionally, the cobalt (Co) composition, commonly used as a metallic binder in the sintering of PCD, remained stable in both samples at approximately 4 %. This stability indicates that the metallic structure of the material was not significantly altered by femtosecond laser irradiation. Carbon (C), the primary component of PCD, was detected at levels between 75 % and 80 % in the sample before laser exposure and remained virtually unchanged after irradiation, reinforcing the conclusion that the diamond structure was preserved.

3.2. Post-machining textures

Most of the cutting tools tested with textures oriented parallel to the cutting edge broke near the cutting edge. In contrast, those with perpendicular textures produced less noise during turning compared to smooth tools. These findings differ from the conclusions of the review conducted by Gajrani e Sankar [46], which stated that textures may not impact the mechanical strength of cutting tools. There is a clear correlation between parameters such as material hardness, ductility, tool strength, and texture dimensions.

As observed in the literature, the study by Dhage et al. [47] specifies that, tribologically, the optimal direction for a linear groove texture is perpendicular to the chip flow (parallel to the cutting edge). This orientation reduces the contact area between the chip and the tool. They argue that, in cases where grooves are perpendicular to the cutting edge, chips may obstruct the texture, leading to increased contact. However, these authors worked with carbon steel, which is not as ductile as aluminum. Several authors who agree with Dhage et al. [47] also studied materials that are not highly ductile [28,29,48,49].

On the other hand, Kang et al. [26], who worked with aluminum, found that the direction of grooves perpendicular to the cutting edge yields better results (lower cutting forces and adhesion effects) compared to grooves parallel to the cutting edge. The results obtained in this study corroborate the findings by [26].

The issue encountered when machining aluminum with textures parallel to the cutting edge was the adhesion (sticking) of aluminum within the grooves, generating significant stresses on the texture surfaces. This occurs due to friction between the stationary aluminum inside the texture and the forming chips, resulting in substantial stresses. In the case of textures parallel to the cutting edge, the anchoring effect of the material on the cutting tool is intensified, leading to the formation of cracks. Textures acted as stress accumulators within the cutting tool structure, exacerbating the problem of crack formation, and this phenomenon is worsened for textures parallel to the cutting edge. The distance between the start of the textures and the cutting edge impacts the structural strength of the PCD, and after turning, it is evident that tools with grooves parallel to the cutting edge require a greater distance to avoid such cracks. Even in the case of smaller texture dimensions (Type PA45), some grooves formed at higher cutting speeds. In Fig. 9, these events can be observed.

Analyzing studies that investigated the behavior of different materials under the same machining conditions using textured tools, such as [50,51] and [52], reveals a correlation between the ductility of materials and their response to textured tools. Unlike ductile materials, in the machining of brittle and hard materials, the chip material struggles more to deform and reach the bottom of the texture. However, tool wear allows the chip to penetrate deeper into the texture, ensuring that the lubricant stored within comes into contact with the chip flow, contributing to the cutting process. On the other hand, when using tools that do not wear significantly, as in the machining of aluminum with PCD tools, this process does not occur. However, due to the high ductility of aluminum, the chip deforms sufficiently to partially enter the texture and contact the lubricant stored within, allowing the chip to continue flowing with reduced friction. Such a phenomenon also minimizes the material adhesion effect on the cutting tool.

Regarding the effect of MoS_2, no visible influence on chip morphology was observed. The most noticeable impact attributable to MoS_2 is the significant reduction of chip adhesion within the textured regions. This indicates that the solid lubricant effectively prevents aluminum from anchoring to the tool surface, particularly within the grooves, thereby contributing to improved tribological behavior during machining.

Fig. 8 presents images with higher clarity of the textured surface after turning, clearly showing the residual presence of MoS_2 and aluminum inside the grooves. This confirms that a portion of the solid lubricant remains on the tool surface after chip contact, contributing to the

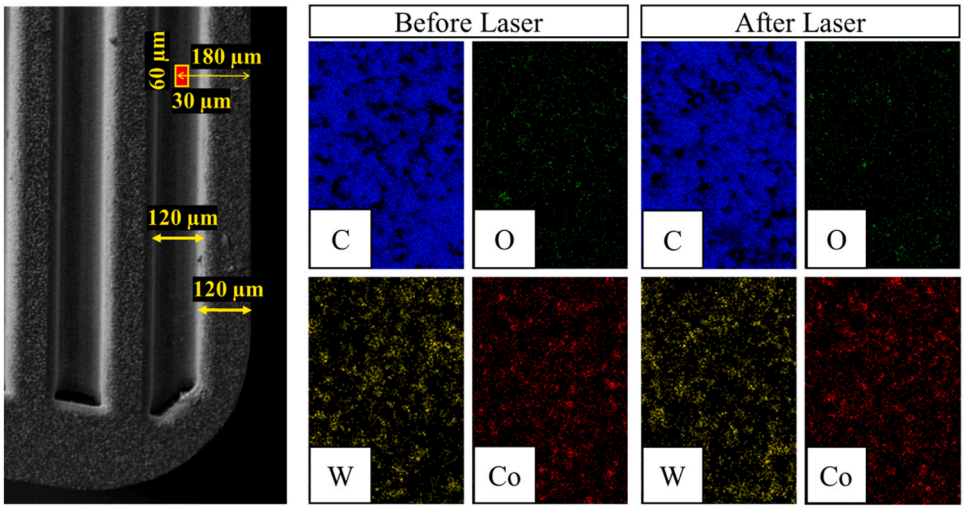

Fig. 7. On the left is the scanning electron microscopy (SEM) image indicating the area (red rectangle) where EDS analysis was performed after laser texturing. On the right are the results of the chemical composition spectrum in a cutting tool surface before and after the femtosecond laser irradiation, covered an area of 30 × 60 µm. Blue represents carbon, green represents oxygen, yellow represents tungsten, and red represents cobalt.

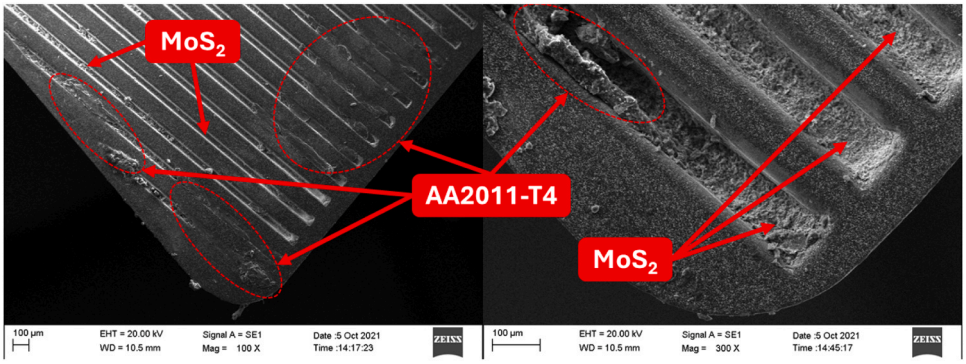

Fig. 8. SEM images of the textured surface after machining with MoS_2 lubrication. The presence of residual MoS_2 is visible inside the grooves, indicating that the solid lubricant remains partially embedded in the texture even after the cutting process. This visual evidence supports the role of MoS_2 in reducing material adhesion on the tool surface. The adhesion of aluminum is also evidenced.

reduction of material adhesion.

Fig. 9 allows for a comparison of the presence and absence of MoS_2 for all types of textures (all cutting tools in the figure were used under the same cutting condition, with a cutting speed of 400 m/min). The perceptible presence of aluminum, highlighted by its typical color, can be observed. In the rest of the texture, residues of solid lubricant (with its silicone sealant) are visible.

To quantify the effect of MoS_2 on reducing material adhesion, an analysis of the aluminum-adhered area within the textures was performed, comparing conditions with and without solid lubricant. Fig. 9, PA120 line, was used as a reference to illustrate the measurement method of the adhered area. From the post-machining images, it was possible to estimate the average reduction in adhesion area for each tested condition. The results showed reductions of 9.07 % for PA45, 38.52 % for PE45, 60.47 % for PA120, and 89.12 % for PE120, indicating that larger textures and those perpendicular to the cutting edge are more effective in reducing adhesion when filled with MoS_2.

A change in the chip-tool contact length is also observed. From the perspective of machining mechanics, a reduction in chip-tool contact length is typically expected to influence chip morphology, as described by classical models such as Merchant and Oxley [53]. However, when comparing chips produced by textured tools with and without solid lubrication, no significant differences were observed in chip thickness or curvature. Considering the image scale, the contact length reduction caused by lubrication was only a few micrometers, which explains the lack of observable variation in chip morphology.

The synergistic friction reduction observed with the combination of surface texturing and MoS_2 addition can be attributed to the complementary mechanisms by which each strategy acts at the tool–chip interface. The microtextured grooves serve as reservoirs that store solid lubricant particles, ensuring their sustained presence in the cutting zone even under high-stress machining conditions. As the workpiece material flows over the textured surface, the stored MoS_2 is gradually released and forms a thin, adherent lubricating film along the contact interface. This film, characterized by the lamellar structure and weak interlayer bonding of MoS_2, facilitates easy shear and sliding between the tool and chip, thereby reducing the coefficient of friction more effectively than either texturing or lubrication alone. Additionally, the textures disrupt the continuity of the contact area, minimizing the real area of adhesion and providing escape pathways for wear debris and excess lubricant, which further stabilizes the lubricating action and prevents localized buildup. Similar synergistic effects were reported by Zhang et al. [54], who observed significant friction and wear reduction when applying femtosecond laser texturing and embedding WS_2 solid lubricant in WC/Co TiAlN-coated tools during the turning of AISI 1045 steel. Comparable results were also presented by Xing et al. [55], who used Al_2O_3/TiC ceramic tools with nanotextures and WS_2/Zr embedded soft coatings in both perpendicular and parallel orientations to the cutting

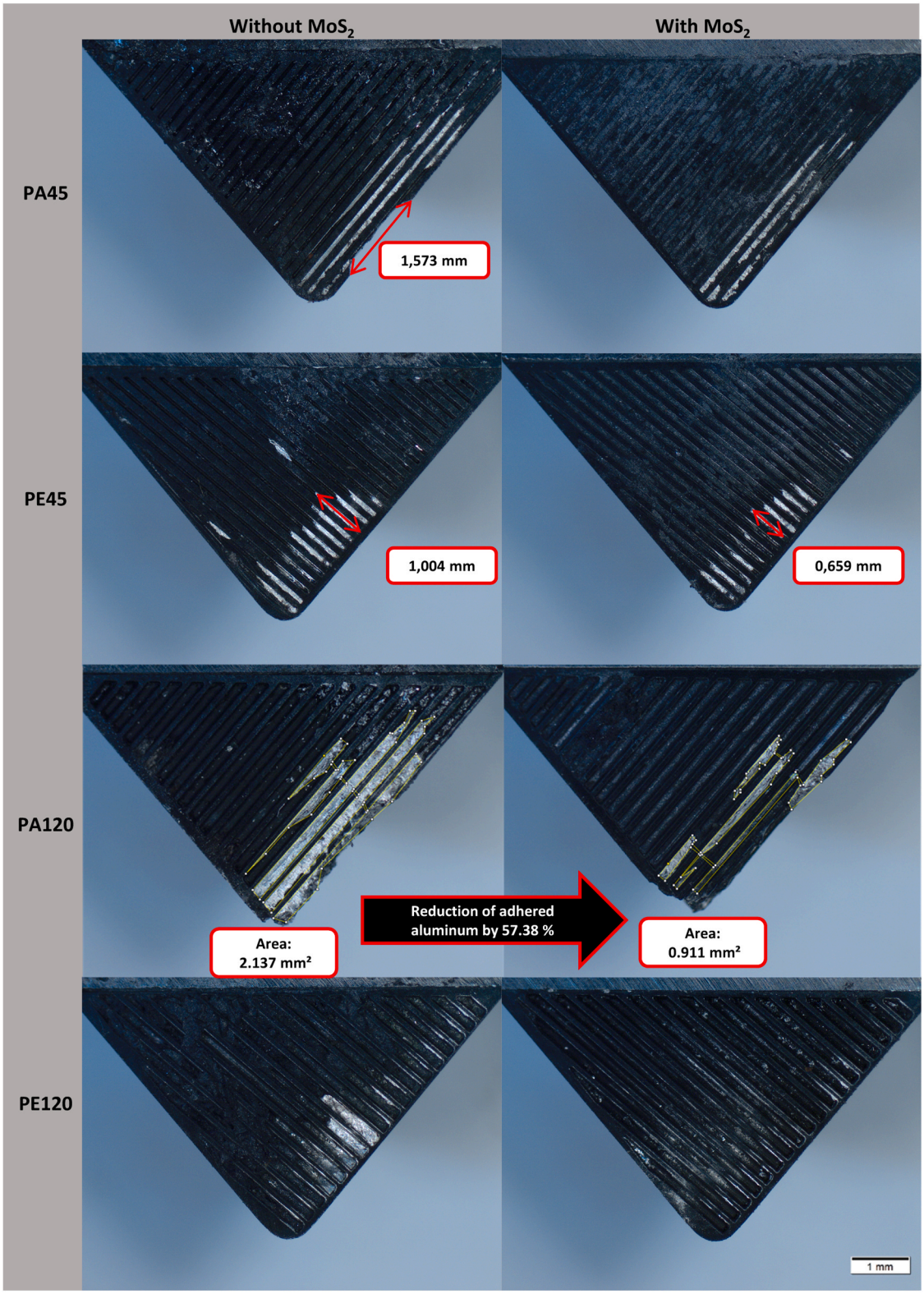

Fig. 9. Surface of cutting tools after machining. Accumulation of aluminum and the presence and/or absence of lubricant can be observed. Turning was performed at a cutting speed of 400 m/min, a relatively aggressive condition. The PA120 texture line illustrates the methodology for measuring the area of aluminum adhered within the textures.

edge for the turning of AISI 1045 steel.

Furthermore, the effectiveness of this synergy is particularly pronounced in highly ductile materials such as aluminum alloys, where chip adhesion and built-up edge formation are common challenges. The presence of MoS_2 within the textured grooves impedes the tendency of aluminum to anchor within the microcavities, as the solid lubricant occupies potential adhesion sites and promotes continuous renewal of the lubricating layer during cutting. This not only reduces friction and

cutting forces but also protects the tool surface from severe adhesive wear and thermal effects. The experimental results—showing significant reductions in both material adhesion and surface roughness, especially for perpendicular textures filled with MoS_2—support this mechanistic interpretation. Comparable findings were also reported by Ahmed and Veldhuis [56], who demonstrated improved tribological performance in the turning of AISI 304 stainless steel using WC-Co tools coated with WS_2, as well as by Xing et al. [55] for ceramic tools with nano-textures and WS_2/Zr coatings. While additional data would further strengthen these conclusions, the observed trends are consistent with established tribological principles and corroborate findings from related literature, reinforcing the credibility of the synergistic effect between surface texturing and solid lubrication.

3.3. Surface roughness of the machined workpiece

The surface roughness of the aluminum bars was evaluated considering the roughness parameters Ra, Rq, and Rz. In Fig. 10, the bars turned with the following types of cutting tools are shown (from left to right): smooth tools, textured tools of type PA45, PE45, PA120, and PE120. A noticeable mark is present at a specific height of the machined surface, where the upper part corresponds to turning at a cutting speed of 200 m/min and the lower part at 400 m/min. A considerable number of burrs are observed on the bar machined with the PA120 texture tool, which experienced edge breakage under all tested conditions.

The significant presence of burrs observed on the workpiece machined using the PA120 tool at 400 m/min in the presence of MoS_2 appears to be directly associated with a crack formation at the tool's main cutting edge. This crack was likely induced by surface stresses concentrated around the textured region, which in this case is parallel to the cutting edge. Such an orientation can act as a stress concentrator, especially under severe cutting conditions, promoting crack initiation and propagation.

Notably, this particular condition combines several critical factors: the highest cutting speed tested (400 m/min), the largest texture dimension (120 μm), and the most mechanically unfavorable groove orientation (parallel to the cutting edge, i.e., perpendicular to chip flow). These factors synergistically increase the mechanical loading on the tool's textured region, making it more susceptible to structural failure and, consequently, impairing the quality of the machined surface through burr formation.

The surface roughness results of the aluminum bars machined with smooth and textured tools are shown in Fig. 11 for a cutting speed of 200 m/min and in Fig. 12 for a cutting speed of 400 m/min. Only the tool with PE45 textures at a cutting speed of 200 m/min and the PE120

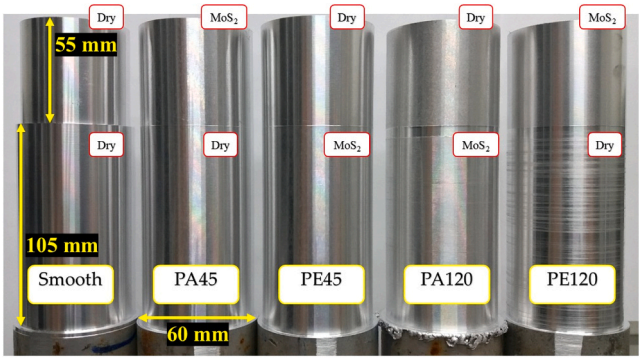

Fig. 10. Illustration of the visual overview of the surfaces of the turned bars. The initial diameter of the bar is approximately 60 mm. The upper part corresponds to turning with a cutting speed of 200 m/min, and had a cutting length of approximately 55 mm. The lower part corresponds to a cutting speed of 400 m/min and a cutting length of 105 mm. The presence or absence of MoS_2 is indicated for each condition.

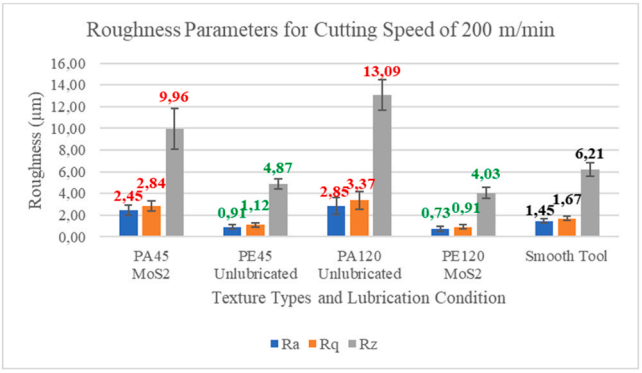

Fig. 11. Average roughness parameters of the bars machined with each type of tested cutting tool at a cutting speed of 200 m/min.

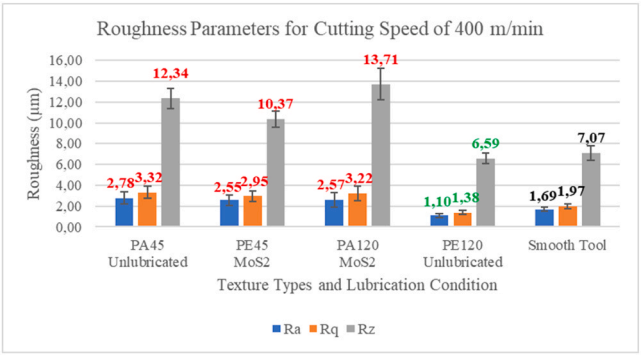

Fig. 12. Average roughness parameters of the bars machined with each type of tested cutting tool at a cutting speed of 400 m/min.

textures at both studied cutting speeds reduced surface roughness compared to smooth tools (without textures).

The greatest improvement in roughness (Ra) was observed with the PE120 texture filled with MoS_2, achieving a reduction of 49.65 % compared to a non-textured tool. This improvement is more than double that reported by Jesudass e Kalaichelvan [57], who found a 23.21 % reduction in roughness when turning aluminum with dimple-type textures. In contrast, the study by Sun et al. (2016) [20], which also turned aluminum with groove textures, reported a Ra reduction of 43–69 %, a range that encompasses the results obtained in the present work.

Table 5 shows the analysis of variance (ANOVA) of roughness considering all test conditions variables and Fig. 13 presents the Pareto's diagram. Since the three analyzed roughness parameters followed the same trend, only the Ra parameter will be shown. It is evident that the texture direction and cutting speed are significant input variables for the surface roughness of the machined workpiece (p-value < 0.05), with a confidence level of 95 % and a significance level of 5 % (Table 5).

The texture direction, followed by the cutting speed, are the main contributors to the variation in the roughness of the machined workpiece. The texture dimensions and lubrication condition did not significantly influence roughness. However, the excessively discrepant results

Table 5
ANOVA for Roughness (Ra) of the Machined Workpiece.

Factor	S.Q.	G.L.	F	p-value
Texture Direction	10.77360	1	51.07054	< 0.000001
Dimensions	0.77760	1	3.68609	0.070010
Cutting Speed	1.59135	1	7.54354	0.012831
Lubrication Condition	0.16335	1	0.77433	0.389874
Error	4.00815	1		
Total S.Q.	17.31405	5		

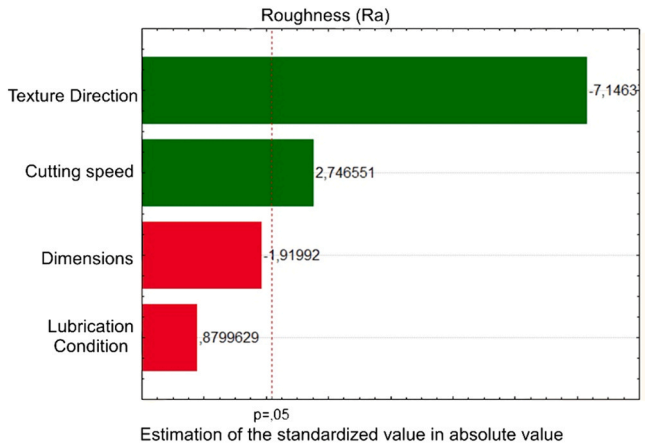

Fig. 13. Pareto diagram of Ra roughness for the variables in all test conditions.

of the PA120 texture mask the effects of other parameters. The large amount of burrs found exclusively on the bar turned with the PA120 texture reinforces this idea (Fig. 10). Thus, a new Pareto diagram was created, excluding the PA120 texture. The new diagram revealed a different result for the significance of the Ra variable on roughness (Fig. 14).

With the new Pareto diagram, it is observed that all input variables significantly influence the final roughness of the turned workpiece. The texture direction parameter aligns with other analyses, with the direction perpendicular to the cutting edge being the most favorable. Regarding the influence of texture dimensions, there are few references in the literature showing this effect on roughness for groove textures. Generally, references focus more on dimple texture dimensions for analyzing roughness in aluminum workpieces. Therefore, to evaluate the effect of each parameter, trend graphs were generated, as shown in Fig. 15 and Fig. 16.

Fig. 15 clearly shows a trend of reduced roughness with increasing texture dimensions for both cutting speeds tested. A possible explanation for this phenomenon is that larger textures promote chip frequency and fragmentation, which aids in heat dissipation and prevents workpiece overheating. Continuous chips may be entangled, whereas segmented chips improve evacuation and prevent damage to the final workpiece. Textures also allow the chip to deform gradually according to its geometry, resulting in a smoother cutting process and improved surface integrity of the final workpiece.

The Fig. 16 shows that the presence of solid lubricant, contrary to expectations, increased the Ra roughness of the workpieces, even

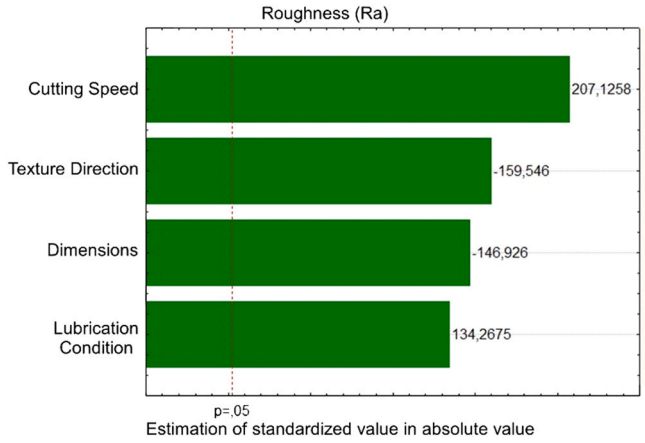

Fig. 14. Pareto diagram of Ra roughness for the variables excluding tests with PA120 textures.

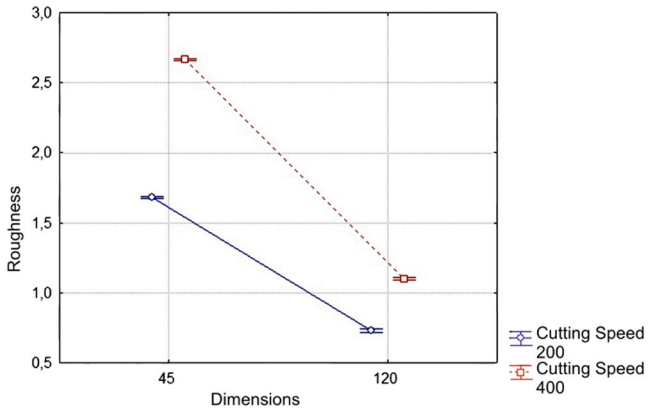

Fig. 15. Influence of texture dimensions on roughness (Ra) for the two tested cutting speed conditions.

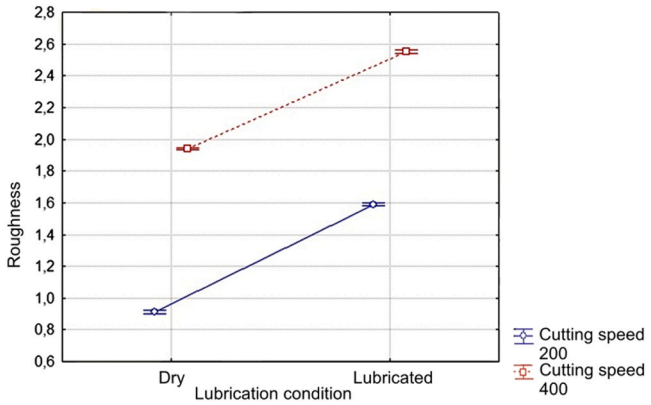

Fig. 16. Influence of MoS_2 presence in textures on roughness (Ra) for the two tested cutting speed conditions.

though the significance factor p for the lubrication condition was the lowest in the analysis. These results exclude tests with PA120 textured tools, emphasizing the influence of smaller textures, PA45 and PE45. In these smaller textures, the use of solid MoS_2 lubricant fills the texture in such a way that aluminum adhesion inside the texture is not favored, which may have hindered chip sliding and resulted in increased roughness. This is more evident at the lower cutting speed of 200 m/min, as shown in Fig. 16.

The presence of MoS_2 positively contributed to reducing the adhesion of chips anchored within the textures, thereby helping to decrease material buildup on the tool surface. However, the application of MoS_2, fixed by silicone, also resulted in an effective reduction of the available volume within the texture grooves due to partial filling of these spaces. As observed in the results, larger textures yield better outcomes in terms of surface roughness, indicating that the free volume within the texture is a critical factor for its functional performance.

Therefore, it is plausible that the presence of MoS_2 limited the effective dimensions of the textures, causing an effect similar to a reduction in their size or depth, which compromised the expected benefits of solid lubrication. In other words, the positive effect of chip adhesion reduction did not compensate for the loss of functional texture volume, resulting in overall inferior surface roughness performance.

This behavior may be particularly pronounced at high cutting speeds, where the formation of a stable lubricating film becomes more difficult, reducing the effectiveness of MoS_2. Hence, a potential solution to mitigate this issue would be to increase the depth of the textures, allowing adequate volume for housing the solid lubricant, thereby maintaining its benefits without compromising the functional space of

the texture.

As shown in the surface roughness results, all textures with grooves parallel to the cutting edge (PA) led to a deterioration in surface finish. This orientation places the grooves perpendicular to the chip flow direction, which, in the case of aluminum, tends to promote chip entrapment and hinder evacuation, negatively affecting the surface quality. This behavior is consistent with findings reported in the literature (and commented in the manuscript) for aluminum alloys [26], although opposite effects have been observed when applying the same texture patterns to other materials [28,29,47–49]. Additionally, as highlighted in the Pareto analysis, the "groove orientation" factor has a significantly higher statistical impact than the presence of MoS_2, which explains the performance differences between PE and PA despite similar lubricant volumes.

4. Conclusions

This study investigated the application of femtosecond laser machining for the microtexturing of polycrystalline diamond (PCD) tools, yielding the following key conclusions:

1. Process Integrity, Debris Management, and Cleaning: Femtosecond laser parameters enabled the fabrication of textures with high dimensional fidelity and smooth profiles without inducing thermal or cumulative damage to the PCD surface. No significant graphitization was observed. The process generated minimal debris, which could be effectively removed using non-invasive cleaning methods such as bristle brushes and ultrasonic baths, eliminating the need for abrasive or chemical post-processing.
2. Dimensional Consistency and Laser Path Effects: Both 45 μm and 120 μm textures were successfully produced. The smaller 45 μm textures exhibited greater variation in width-to-depth ratio, with a tendency for width reduction at increased depths, while the 120 μm textures maintained more consistent geometry. An increase in depth was observed at the end of the texture paths (last 0.5 mm), attributed to reduced laser scanning speed, with depth increases of 11 % and 25 % for 45 μm and 120 μm textures, respectively.
3. Impact of Texture Parameters and Lubrication on Machining Performance: Texture orientation and dimensions significantly influenced tool performance during the machining of aluminum. Textures aligned perpendicular to the cutting edge (parallel to chip flow) improved surface roughness and reduced material adhesion, whereas parallel alignments could negatively affect tool performance and, in some cases, induce structural damage, particularly with larger textures. The combination of the PE120 texture with MoS_2 lubrication produced the greatest improvement in surface finish, resulting in a 49 % reduction in the Ra parameter.

These findings support the potential of femtosecond laser texturing for enhancing the tribological performance of PCD tools, particularly when texture dimensions and orientations are optimized and used with appropriate lubrication. Future studies should include simulation, experimental strength analyses and chip imaging to further investigate the reliability of textured tools and the effects of solid lubrication on chip–tool interactions.

Declaration of Generative AI and AI-assisted technologies in the writing process

During the preparation of this work the authors used, with caution, the chatbot Chat GPT developed by OpenAI, to improve language and readability. After using this tool, the authors reviewed and edited the content as needed and take full responsibility for the content of the publication.

Declaration of Competing Interest

The authors declare that they have no known competing financial interests or personal relationships that could have appeared to influence the work reported in this paper.

Acknowledgments

The authors thank the technical support provided during the experiments by the Laboratory for Teaching and Research in Machining (LEPU) at the Federal University of Uberlândia (UFU), MG Brasil, and the Nuclear and Energy Research Institute (IPEN), as well as MAPAL do Brasil Ferramentas de Precisão Ltda for supplying the tooling. They also acknowledge the financial support from Brazilian research agencies: CNPq, FAPEMIG, and the Coordination for the Improvement of Higher Education Personnel - Brazil (CAPES) - Financial Code 001.

References

[1] Lima MSFD. Laser beam welding of titanium nitride coated titanium using pulse-shaping. Mater Res 2005;8:323–8. https://doi.org/10.1590/S1516-14392005000300017.
[2] Machado AR, da Silva LR, de Souza FC, Davis R, Pereira LC, Sales WF, Ezugwu EO. State of the art of tool texturing in machining. J Mater Process Technol 2021;293:117096. https://doi.org/10.1016/j.jmatprotec.2021.117096.
[3] Samad RE, Machado LM, Vieira Jr ND, De Rossi W. Ultrashort laser pulses machining. Laser Pulses-Theory Technol Appl 2012:143–74. https://doi.org/10.5772/46235.
[4] Preuss S, Demchuk A, Stuke M. Sub-picosecond UV laser ablation of metals. Appl Phys A 1995;61:33–7. https://doi.org/10.1007/BF01538207.
[5] Krueger J, Kautek W. Femtosecond-pulse laser processing of metallic and semiconducting thin films. Laser-Induced Thin Film Processing, 2403. SPIE; 1995. p. 436–47. https://doi.org/10.1117/12.206276 (April).
[6] Fermann ME, Galvanauskas A, Sucha G, editors. CRC Press; 2002. https://doi.org/10.1201/9780203910207. Ultrafast lasers: technology and applications.
[7] Fork RL, Greene BI, Shank CV. Generation of optical pulses shorter than 0.1 psec by colliding pulse mode locking. Appl Phys Lett 1981;38(9):671–2. https://doi.org/10.1063/1.92500.
[8] Stuart BC, Feit MD, Rubenchik AM, Shore BW, Perry MD. Laser-induced damage in dielectrics with nanosecond to subpicosecond pulses. Phys Rev Lett 1995;74(12):2248. https://doi.org/10.1103/PhysRevLett.74.2248.
[9] Kautek W, Krüger J, Lenzner M, Sartania S, Spielmann C, Krausz F. Laser ablation of dielectrics with pulse durations between 20 fs and 3 ps. Appl Phys Lett 1996;69(21):3146–8. https://doi.org/10.1063/1.116810.
[10] Ogawa Y, Ota M, Nakamoto K, Fukaya T, Russell M, Zohdi TI, Aoyama H. A study on machining of binder-less polycrystalline diamond by femtosecond pulsed laser for fabrication of micro milling tools. CIRP Ann 2016;65(1):245–8. https://doi.org/10.1016/j.cirp.2016.04.081.
[11] Sotillo B, Bharadwaj V, Hadden JP, Rampini S, Chiappini A, Fernandez TT, Eaton SM. Visible to infrared diamond photonics enabled by focused femtosecond laser pulses. Micromachines 2017;8(2):60. https://doi.org/10.3390/mi8020060.
[12] White YV, Parrish M, Li X, Davis LM, Hofmeister W. Femtosecond micro-and nano-machining of materials for microfluidic applications. Nanoengineering: Fabrication, Properties, Optics, and Devices V, 7039. SPIE; 2008. p. 71–80. https://doi.org/10.1117/12.799855 (September).
[13] Yang Y, Zhao G, Hu M, Li L, He N, Jamil M. Fabrication of CVD diamond micro-milling tool by hybrid machining of laser-induced graphitization and precision grinding. Ceram Int 2019;45(18):24127–36. https://doi.org/10.1016/j.ceramint.2019.08.121.
[14] Vignesh G, Barik D, Ragupathi P, Aravind S. Experimental analysis on turning of AISI 4340 steel using non-textured, dimple textured and MoS2 coated dimple textured carbide cutting inserts at the rack surface. Mater Today Proc 2020;33:2616–20. https://doi.org/10.1016/j.matpr.2020.01.125.
[15] Dheeraj N, Sanjay S, Bhargav KK, Jagadesh T. Investigations into solid lubricant filled textured tools on hole geometry and surface integrity during drilling of aluminium alloy. Mater Today Proc 2020;26:991–7. https://doi.org/10.1016/j.matpr.2020.01.163.
[16] Ze W, Jianxin D, Yang C, Youqiang X, Jun Z. Performance of the self-lubricating textured tools in dry cutting of Ti-6Al-4V. Int J Adv Manuf Technol 2012;62:943–51. https://doi.org/10.1007/s00170-011-3853-x.
[17] Feng Y, Zhang J, Wang L, Zhang W, Tian Y, Kong X. Fabrication techniques and cutting performance of micro-textured self-lubricating ceramic cutting tools by in-situ forming of Al2O3-TiC. Int J Refract Met Hard Mater 2017;68:121–9. https://doi.org/10.1016/j.ijrmhm.2017.07.007.
[18] Orra K, Choudhury SK. Tribological aspects of various geometrically shaped micro-textures on cutting insert to improve tool life in hard turning process. J Manuf Process 2018;31:502–13. https://doi.org/10.1016/j.jmapro.2017.12.005.
[19] Song W, Wang Z, Wang S, Zhou K, Guo Z. Experimental study on the cutting temperature of textured carbide tool embedded with graphite. Int J Adv Manuf Technol 2017;93:3419–27. https://doi.org/10.1007/s00170-017-0683-5.

[20] Sun J, Zhou Y, Deng J, Zhao J. Effect of hybrid texture combining micro-pits and micro-grooves on cutting performance of WC/Co-based tools. Int J Adv Manuf Technol 2016;86:3383–94. https://doi.org/10.1007/s00170-016-8452-4.
[21] Gajrani KK, Sankar MR, Dixit US. Environmentally friendly machining with MoS 2-filled mechanically microtextured cutting tools. J Mech Sci Technol 2018;32: 3797–805. https://doi.org/10.1007/s12206-018-0732-5.
[22] Kelly JF, Cotterell MG. Minimal lubrication machining of aluminium alloys. n. 1-3 J Mater Process Technol 2002;v. 120. https://doi.org/10.1016/S0924-0136(01)01126-8. n. 1-3.
[23] Aluminum Association 2000, Aluminum standards and data. Aluminum Association. Disponível em: ⟨https://www.aluminum.org/aluminum-standards-and-data⟩ (Acessed 08 February 2022).
[24] Yang S, Yu S, He C. The surface integrity of titanium alloy when using micro-textured ball-end milling cutters. Micromachines 2018;10(1):21. https://doi.org/10.3390/mi10010021.
[25] Yang S, Wang T, Ren W, Su S. Micro-texture design criteria for cemented carbide ball-end milling cutters. J Mech Sci Technol 2020;34:127–36. https://doi.org/10.1007/s12206-019-1212-2.
[26] Kang Z, Fu Y, Chen Y, Ji J, Fu H, Wang S, Li R. Experimental investigation of concave and convex micro-textures for improving anti-adhesion property of cutting tool in dry finish cutting. Int J Precis Eng ManufGreen Technol 2018;5:583–91. https://doi.org/10.1007/s40684-018-0060-3.
[27] Wu H, Duong NH, Ma J, Lei S. CEL FEM investigation of effects of microgrooved cutting tools in high speed machining of AISI 1045 steel. International Manufacturing Science and Engineering Conference, 50725. American Society of Mechanical Engineers; 2017. https://doi.org/10.1115/MSEC2017-2932.
[28] Kumar CS, Patel SK. Effect of WEDM surface texturing on Al2O3/TiCN composite ceramic tools in dry cutting of hardened steel. Ceram Int 2018;44(2):2510–23. https://doi.org/10.1016/j.ceramint.2017.10.236.
[29] Grguraš D, Pušavec F. Influence of rake face texturing on machining performance of carbide tools. Procedia CIRP 2019;81:904–7. https://doi.org/10.1016/j.procir.2019.03.224.
[30] Su Y, Li L, Wang G, Zhong X. Cutting mechanism and performance of high-speed machining of a titanium alloy using a super-hard textured tool. J Manuf Process 2018;34:706–12. https://doi.org/10.1016/j.jmapro.2018.07.004.
[31] Hao X, Cui W, Li L, Li H, Khan AM, He N. Cutting performance of textured polycrystalline diamond tools with composite lyophilic/lyophobic wettabilities. J Mater Process Technol 2018;260:1–8. https://doi.org/10.1016/j.jmatprotec.2018.04.049.
[32] Su Y, Li Z, Li L, Wang J, Gao H, Wang G. Cutting performance of micro-textured polycrystalline diamond tool in dry cutting. J Manuf Process 2017;27:1–7. https://doi.org/10.1016/j.jmapro.2017.03.013.
[33] Ghosh P, Pacella M. Effect of laser texturing on the performance of ultra-hard single-point cutting tools. Int J Adv Manuf Technol 2020;106:2635–48. https://doi.org/10.1007/s00170-019-04829-1.
[34] Fang S, Klein S. Surface structuring of polycrystalline diamond (PCD) using ultrashort pulse laser and the study of force conditions. Int J Refract Met Hard Mater 2019;84:105036. https://doi.org/10.1016/j.ijrmhm.2019.105036.
[35] Ali B, Litvinyuk IV, Rybachuk M. Femtosecond laser micromachining of diamond: current research status, applications and challenges. Carbon 2021;179:209–26. https://doi.org/10.1016/j.carbon.2021.04.025.
[36] Zalloum OH, Parrish M, Terekhov A, Hofmeister W. On femtosecond micromachining of HPHT single-crystal diamond with direct laser writing using tight focusing. Opt Express 2010;18(12):13122–35. https://doi.org/10.1364/OE.18.013122.
[37] Kononenko TV, Ralchenko VG, Ashkinazi EE, Polikarpov M, Ershov P, Kuznetsov S, Konov VI. Fabrication of polycrystalline diamond refractive X-ray lens by femtosecond laser processing. Appl Phys A 2016;122:1–6. https://doi.org/10.1007/s00339-016-9683-9.
[38] Haseebuddin MR, Pal Bhaskar, Shanmuganatan SP. Influence of MoS2 nano-filler additions on wear behavior of carbon fiber reinforced epoxy composites. Adv Compos Mater 34 1 2025:34–48.
[39] Kang Z, Jun MBG, Fu Y. Performance of cemented carbide cutting tools with volcano-like texture on rake face. International Manufacturing Science and Engineering Conference, 51388. American Society of Mechanical Engineers; 2018. https://doi.org/10.1115/MSEC2018-6311.
[40] Wei Y, Kim MR, Lee DW, Park C, Park SS. Effects of micro textured sapphire tool regarding cutting forces in turning operations. Int J Precis Eng ManufGreen Technol 2017;4:141–7. https://doi.org/10.1007/s40684-017-0017-y.
[41] Xing Y, Deng J, Wang X, Ehmann K, Cao J. Experimental assessment of laser textured cutting tools in dry cutting of aluminum alloys. J Manuf Sci Eng 2016;138 (7):071006. https://doi.org/10.1115/1.4032263.
[42] Rathod P, Aravindan S. Performance evaluation of novel micro-textured tools in improving the machinability of aluminum alloy (Al 6063. Procedia Technol 2016; 23:296–303. https://doi.org/10.1016/j.protcy.2016.03.030.
[43] Zhu WL, Xing Y, Ehmann KF, Ju BF. Ultrasonic elliptical vibration texturing of the rake face of carbide cutting tools for adhesion reduction. Int J Adv Manuf Technol 2016;85:2669–79. https://doi.org/10.1007/s00170-015-8084-0.
[44] Hatch, J.E. Aluminum: Properties and Physical Metallurgy (American Society for Metals), 1984.
[45] Clark IE, Sen PK. Advances in the development of ultrahard cutting tool materials. Finer Points 1999;11(2):6–8.
[46] Gajrani KK, Sankar MR. State of the art on micro to nano textured cutting tools. Mater Today Proc 2017;4(2):3776–85. https://doi.org/10.1016/j.matpr.2017.02.274.
[47] Dhage S, Jayal AD, Sarkar P. Effects of surface texture parameters of cutting tools on friction conditions at tool-chip interface during dry machining of AISI 1045 steel. Procedia Manuf 2019;33:794–801. https://doi.org/10.1016/j.promfg.2019.04.100.
[48] Chen Y, Guo X, Zhang K, Guo D, Zhou C, Gai L. Study on the surface quality of CFRP machined by micro-textured milling tools. J Manuf Process 2019;37:114–23. https://doi.org/10.1016/j.jmapro.2018.11.021.
[49] Arulkirubakaran D, Senthilkumar V, Chilamwar VL, Senthil P. Performance of surface textured tools during machining of Al-Cu/TiB2 composite. Measurement 2019;137:636–46. https://doi.org/10.1016/j.measurement.2019.02.013.
[50] Kawasegi N, Ozaki K, Morita N, Nishimura K, Yamaguchi M. Development and machining performance of a textured diamond cutting tool fabricated with a focused ion beam and heat treatment. Precis Eng 2017;47:311–20. https://doi.org/10.1016/j.precisioneng.2016.09.005.
[51] Stoeterau RL, Janssen A, Mallmann G. Analysis of dimple textured surfaces on cutting tools. J Braz Soc Mech Sci Eng 2017;39:3989–96. https://doi.org/10.1007/s40430-016-0692-6.
[52] Kawasegi N, Kawashima T, Morita N, Nishimura K, Yamaguchi M, Takano N. Effect of texture shape on machining performance of textured diamond cutting tool. Precis Eng 2019;60:21–7. https://doi.org/10.1016/j.precisioneng.2019.07.007.
[53] Machado Álisson Rocha, et al. Teoria da usinagem dos materiais. Editora Blucher; 2015.
[54] Zhang Kedong, et al. Improving dry machining performance of TiAlN hard-coated tools through combined technology of femtosecond laser-textures and WS2 soft-coatings. J Manuf Process 2017;30:492–501. https://doi.org/10.1016/j.jmapro.2017.10.018.
[55] Xing Youqiang, et al. Cutting performance and wear characteristics of Al2O3/TiC ceramic cutting tools with WS2/Zr soft-coatings and nano-textures in dry cutting. 318.1-2 Wear 2014:12–26. https://doi.org/10.1016/j.wear.2014.06.001.
[56] Ahmed Yassmin Seid, Veldhuis SC. Enhancement of carbide tool performance during dry machining through a combination of laser surface texturing and tungsten disulfide soft coatings. Surf Coat Technol 2021;428:127849. https://doi.org/10.1016/j.surfcoat.2021.127849.
[57] Jesudass Thomas S, Kalaichelvan K. Comparative study of the effect of surface texturing on cutting tool in dry cutting. Mater Manuf Process 2018;v. 33(n. 6): 683–94. https://doi.org/10.1080/10426914.2017.1376070.